Formation of Polybrominated Dibenzofurans from Polybrominated Biphenyls

Mohammednoor Altarawneh*†, Bogdan Z. Dlugogorski

School of Engineering and Information Technology
Murdoch University, Perth, Australia

*Corresponding Author:
Phone: (+61) 8 9360-7507
E-mail: M.Altarawneh@Murdoch.edu.au

† On leave from Chemical Engineering Department, Al-Hussein Bin Talal University, Ma'an, Jordan

Abstract

Decades after phasing out their production and use as brominated flame retardants (BFRs), polybrominated biphenyls (PBBs) still pose serious environmental and health problems. The oxidation of PBB has been hypothesised as a pathway for the formation of the notorious polybrominated dibenzofurans (PBDFs) and their dispersion in the environment. However, the exact reaction corridor remains misunderstood, with the existing mechanisms predicting the reaction to proceed via a high energy process that involves the breakage of C-C linkage (~ 118.0 kcal/mol) and the subsequent formation of bromophenols molecules, where the latter are supposed to act as precursors for the formation of PBDFs (~ 40.0 kcal/mol -60.0 kcal/mol). Herein, we show that PBBs produce PBDFs in a facile mechanism through a series of highly exothermic reactions (i.e. overall barriers reside 8.2 kcal/mol – 10.0 kcal/mol below the entrance channel). While the fate of the ROO-type intermediates in oxidation of all aromatics is to emit CO or CO_2, PBDFs constitute the dominant products from the oxidation of PBBs. We have shown that the initially formed R-OO adduct evolve in a very exoergic mechanism to yield PBDFs. In view of the facile oxidative transformation of PBBs into PBDFs, we conclude that is unsafe to dispose BFRs in oxidation processes, as this practice generates high yields of toxic PBDFs.

Keywords: Brominated Flame Retardants (BFRs); Polybrominated Biphenyls (PBBs); Bolybrominated Dibenzofurans (PBDFs); DFT.

1. Introduction

Introduced in 1970s as ingredients in formulations of brominated flame retardants (BFRs), polybrominated biphenyls (PBBs) remain ubiquitous in humans, wildlife and all environmental media (Wei et al. 2012). PBBs also occur as major impurities in technical mixtures of other BFRs, such as polybrominated biphenyl ethers (PBDEs) (Yang et al. 2012). A contamination accident in Michigan in 1973 sensitised the public to the health and environmental toxicity of PBBs, prompting their production phase-out (Hites 2005). Recently, these chemicals have returned into the environmental spotlight, as a consequence of the renewed and mounting concerns relating to their role in formation of other brominated pollutants (Wäger et al. 2011, Blum et al. 2012). Despite the prohibition on their production, PBBs remain in BFRs-laden materials. Uncontrolled burning and incineration constitute the major route for disposal of discarded household item, and an emission source of brominated persistent organic compounds (POPs), including PBBs, into the environment (Davis et al. 2012). Another source of PBBs involves direct gaseous and particle-bound emissions, similarly to the well-studied liberation of PBDE from consumer products (Björklund et al. 2012).

The tendency of PBBs to form the notorious polybrominated dibenzofurans (PBDFs) has added another environmental burden to the hazardous nature of PBBs. Particularly, it has been well established that, oxidation/thermolysis of PBBs generate appreciable amounts of PBDFs (O'Keefe 1987, Thoma et al. 1987, Zacharewski et al. 1988, Luijk and Govers 1992). This route is practically important, as most countries dispose their combustible waste in municipal waste incinerators for energy recovery or in uncontrolled combustion by backyard burning.

Despite recent efforts devoted to gaining understanding of the fate and transformations of PBBs in the environment, including their behaviour in combustion systems, chemical phenomena governing conversion of PBBs into PBDFs remain rather poorly understood. The existing mechanisms incorporate pathways that proceed by high energy steps. These pathways involve formation of precursors (typically bromophenols, bromophenoxys and bromobenzenes) via rupture of the C-C bridge, subsequent coupling of these precursors into PBDFs, followed by HBr intramolecular elimination, oxygen insertion and cyclisation into PBDFs (Weber and Kuch 2003). Our calculated C-C bond fission in a biphenyl molecule amount to 117.8 kcal/mol making this route practically unfeasible. Furthermore, formation of PBDFs from self-condensation of bromophenoxy radical encounters reactions barriers for several individual steps in the range of 40.0 – 60.0 kcal/mol (Yu et al. 2011).

Existing mechanisms are merely hypothesised based on generic schemes involving other halogenated pollutants, rather than being derived from understanding of precise atomic-based descriptions. In our recent study (Altarawneh and Dlugogorski 2013), we have addressed one of the most intriguing questions on how polybrominated diphenyl ethers (PBDEs) transform into PBDD/Fs. We have demonstrated that the overall reaction of triplet oxygen molecule with PBDEs proceed in a complex, nevertheless very exoergic, mechanism to produce PBDDs. In the present investigation, we apply quantum chemistry and transitional state/RRKM theories to provide detailed mechanistic and kinetic insight into the formation of PBDFs from PBBs. As the 2,2'-dibromobiphenyl (**2,2'-DBB**) molecule contains ortho bromine and hydrogen substituents at the two phenyl rings, it is selected as a representative model compound for all congeners of PBBs, to address the atomic-type substitution on prominent coupling/cyclisation reactions. We illustrate a facile route that satisfactorily accounts for the high yield of PBDFs from PBBs, demonstrating that the initial reaction

(phenyl-type radical + O_2) advances in an intricate and highly exoergic mechanism to yield PBDFs.

2. Computational details

Calculations of electronic structures relied on the Gaussian 09 suite of programs (Frisch et al 2009), and involved M05-2X/GTLarge//M05-2X/6-311+G(d,p) level of theory. The meta hybrid M-052X performs well in general applications to predict thermochemistry and kinetics of gas phase systems, although, in specific applications, it can be outperformed by more recently developed functionals (Zhao et al. 2006). We evaluated the rate constants at the high-pressure limit for all reactions. A one-dimensional Eckart functional provided estimations of plausible contribution of quantum tunnelling to values of reaction rate constants. Methodology suggested by (Chandra and Sreedhara Rao 1997) served to estimate barrier widths. Table 1 lists fitted rate constants for all reactions in both directions forward and reverse, at the high-pressure limit. We solved the time-dependent master equation within the formalism of the RRKM theory (Klippenstein 2003) to determine pressure-dependent rate constants for prominent reactions at 1.0 atm. Equilibrium calculations of the Master RRKM equation comprised an exponential-down model with ΔE_{down} = 800 cm^{-1}, an energy increment of 100 cm^{-1}, and nitrogen chosen as a bath gas to simulate moderate collision conditions. We set the Lennard-Jones parameters for the reactive species to α = 7.0 Å and k/ε_b = 500.0 K, with modified Arrhenius parameters, at 1.0 atm, assembled in Table 2. Finally, calculations performed with the ChemRate code (Mokrushin 2002) yielded the reaction rate constants. The effect of the size of the integration grid on the M052X energies was found to be minimal for calculations deploying more than 99 and 590 radial and angular points, respectively.

3. Results and discussions

The **2,2'-DBB** molecule possess three distinct bonds, namely C-H, C-Br and C-C. Calculated dissociation energies for these bonds amount to 112.3 kcal/mol, 83.0 kcal/mol and 118.5 kcal/mol, respectively. With these high endoergic values, unimolecular decomposition of the **2,2'-DBB** molecule via the bond fission appears as an unviable reaction corridor at all temperatures. However, the **2,2'-DBB** molecule reacts readily with H, OH, Br, HO_2 radicals under conditions encountered in typical combustion environment. For instance, in Figure 1, we demonstrate that the most plausible reactions of the H atoms with the **2,2'-DBB** molecule take place through inconsequential enthalpy barriers within the range of 7.0 kcal/mol – 10.1 kcal/mol. BFRs-containing materials (i.e., polymers with BFRs additives) act as effective sources of hydrogen atoms. Thus, the decomposition of polymeric matrices induces the initial reactions of PBBs with H atoms. With the presence of H and Br atoms on the aromatic ring, reactions of the **2,2'-DBB** molecule with H and OH radicals take place with different selectivity. OH radicals preferentially abstract H atoms rather than Br atoms, whilst H atoms preferentially abstract Br atoms from the aromatic ring (Altarawneh and Dlugogorski 2013).

Figure 2 depicts detailed energetic profiles for the formation of dibenzofuran (**DF**) and 1-monobromodibenzofuran (**1-MBDF**) from the initial oxidation of the **2,2'-DBB** molecule. Bimolecular reactions of the **2,2'-DBB** molecule with active radicals in the combustion system produce the phenyl-type radical **M1**. Addition of the oxygen molecule to the **M1** radical liberates 45.6 kcal/mol of excess energy and results in the formation of the peroxy-type radical **M2**. The calculated well-depth of the **M1** + O_2 reaction matches very well the corresponding value for the oxygen addition to a phenyl radical, i.e, 48.6 kcal/mol (da Silva and Bozzelli 2008). **M2** could also arise as a result of a triplet oxygen molecule displacing a

Br atom via the transition structure **TS1** (43.9 kcal/mol) and a reaction exoergecity of 39.0 kcal/mol. However, this addition/elimination reaction is largely reversible as the rate constant for the reverse reaction exceeds that of the forward reaction by several orders of magnitudes at all temperatures. Unimolecular isomerisation of M2 into the 1,1-dioxiranyl-type (**M5**) and the 1,2-dioxetanyl-type (**M4**) radicals demands activation energies of 26.4 kcal/mol (**TS3**) and 47.4 kcal/mol (**TS2**). Alternatively, the outer-peroxy atom departs the **M2** adduct via the general reaction (ROO + R`H → ROOH + R` → RO + OH + R`) or through barrierless bond fission with endogercity of 37.4 kcal/mol to produce the phenoxy-type radical of M13. The calculated O-O bond dissociation in the **M2** radical concurs with a literature corresponding value (da Silva and Bozzelli 2008) for the phenylperoxy radical, i.e, 37.2 kcal/mol at the O3LYP/6-31G(d) theoretical level and our own CBS-QB3 calculations at 38.1 kcal/mol.

The **M13** radical branches into three channels, namely, ring-closure reactions into a DF molecule and the **M14** radical and a ring-contraction into the **M15** adduct. Self-ejection of the out-of-plane H atom in the **M14** intermediate produces the 4-MBDF molecule through a reaction barrier of 23.6 kcal/mol (**TS8**). Calculated reaction rate constants given in Table 1 indicate that the two pathways, leading to the formation of the **DF** (**M13 → DF** + Br) and **1-MBDF** (**M13 → M14 → 4-MBDF +** H)**,** exhibit comparable reaction rate constants at temperature relevant to the formation of PBDFs; i.e., 600 K – 1200 K. Ring-contraction of **M13** appears unimportant in view of the sizable energy barrier embedded in **TS7** (48.0 kcal/mol).

Isomerisation of **M2** into **M3** marks the lowest energy barrier among the four plausible unimolecular exit channels for **M2**. This process comprises the transition structure **TS4** in

which the outer-oxygen atom in the peroxy group bridges onto the pivot carbon atom of the other phenyl ring:

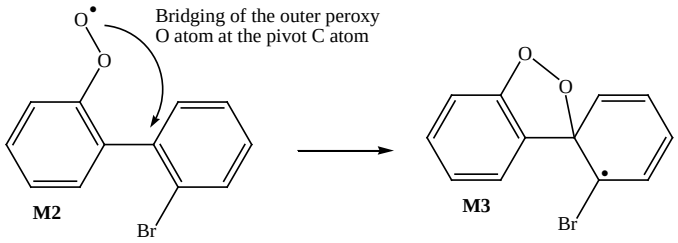

Barrier height of **TS4** amounts to 21.9 kcal/mol. Figure 3 portrays branching ratios for the two most accessible exit channels for M2, i.e., **M2** → **M3** and **M2** → **M3** at the high-pressure limit. At temperature as high as 1170 K, formation of the **M3** intermediate holds more importance than formation of the **M5** radical. Ring opening in the **M5** radical along the reaction (**M5** → **M16**) demands activation energy of 68.1 kcal/mol and produces the **M16** intermediate. Further decomposition of **M16** is most likely to proceed via expulsions of CO_2 two C_2H_2 molecules forming a 1-bromophenyl radical. Investigation of these pathways is beyond the scope of this study.

The three-membered ring structure of **M3** yields two oxirane-type conformations (**M6** and **M7**) through comparable reaction barriers of 25.3 kcal/mol (**TS10**) and 23.5 kcal/mol (**TS9**), in that order:

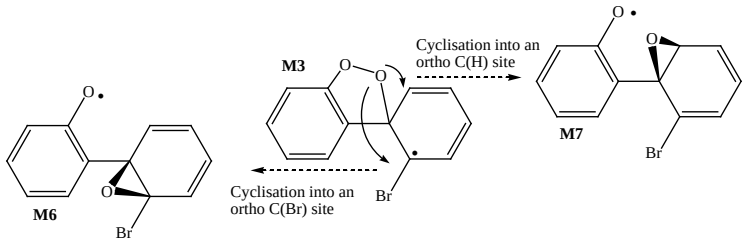

The two oxirane-type structures **M6** and **M7**reside in an energy well-depth at 29.6 kcal/mol and 26.7 kcal/mol with respect to **M3**, respectively. Based on calculated rate constants in

Table 1, it is evident that the kinetics of the cyclisation reaction is somewhat insensitive to the atomic substitution on the other phenyl ring (i.e., Br versus H) as the formation rates of **M6** and **M7** are within factors of 3.0 – 3.4 throughout the considered temperature interval. Ring-closure reaction in **M7** adduct via **TS11** results in simultaneous ejection of a Br atom and the formation of oxirane-type structure of M11. Self-expulsion of the oxiranyl O atom in **M11** is regarded a spin-forbidden reaction. Instead, the **M11** intermediate could react with reactive radicals through its oxiranyl O atom. Herein, we consider the formation of the **M12** moeity via addition of Br atom to the oxiranyl O atom. This reaction demands an activation energy of 9.0 kcal/mol (**TS17**) and it is associated with a moderate exoergecity of 12.4 kcal/mol. In the final step, the out-of-palne BrO moiety departs the **M12** structure to yield a DF molecule through an activation barrier of 17.3 kcal/mol (**TS18**). The enolisation step from **M7** to **M9** should be hindered in view of the sizable energy barrier of **TS13** (70.4 kcal/mol) in reference to the competing cylisation reaction leading to formation of **M11**.

Analogously, subsequent reactions toward the generation of **1-MBDF** molecule involve cyclisation (i.e., **M6** → **M8**), H-transfer (i.e., **M8** → **M10**), and expulsion of the out-of-plane OH group (i.e., **M10** → **1-MBDF** + OH). All these reactions display exoergicity, demanding modest reaction barriers. The overall barriers of the conversion of M3 into DF and 4-MBDF reside below the initial separated reactants (O_2 and **M1**) by 8.2 kcal/mol (**TS9**) and 10.0 kcal/mol (**TS10**), respectively. This finding indicates the spontaneous nature of the potential energy surface leading to the formation of **DF** and **1-MBDF**.

Based on results from RRKM simulations in Table 2, Figure 4 depicts the Arrhenius plots, at 1.0 atm, for the three opening reactions in conversion of **2,2'-DBB** into **DF** and **1-MBDF**, namely, **M2** → **M3**, **M3** → **M6** and **M3** → **M7**.

The new results presented in this study should be useful to build robust kinetic models for the formation of PBDFs from PBBs. Owing to the similar physical and chemical properties of bromine and chlorine atoms, mechanistic and kinetic data presented herein can also be applied to predict the formation of chlorinated dibenzofurans (PCDFs) from oxidation of chlorinated biphenyls (PCBs) (Thuan et al. 2013). We have demonstrated that, the formation of an ortho-centred phenyl-type radical upon a loss of an ortho H or Br atom paves the way for a facile generation of MBDFs. Atomic-type substitution on the carbons adjacent to the C-C bridge exerts little influence on the feasibility of the mechanism. As molecules of triplet oxygen could "effortlessly" transform PBBs into PBDFs, it is safer and wiser to carry out thermal treatment of municipal wastes under reducing or even under oxygen-deficient conditions.

Appendic A. Supplementary material

Tables S.1, Cartesian coordinates, total energies and vibrational frequencies for all structures. This material is available free of charge via the Internet at http://pubs.acs.org.

Acknowledgements

This study has been funded by the Australian Research Council (ARC) and supported by grants of computing time from the National Computational Infrastructure (NCI) in Canberra as well as from the iVEC supercomputing facilities at Perth.

References

Altarawneh, M. and B. Z. Dlugogorski (2013). A mechanistic and kinetic study on the formation of PBDD/Fs from PBDEs. Environ. Sci.Technol. 47: 5118-5127.

Björklund, J. A., K. Thuresson, A. P. Cousins, U. Sellström, G. Emenius and C. A. de Wit (2012). Indoor air is a significant source of Tri-decabrominated diphenyl ethers to outdoor air via ventilation systems. Environ. Sci. Technol. 46: 5876-5884.

Blum, A., V. Babrauskas and L. Brinbaum (2012). Replacement for pentaPDE flame retardant: is there an improvement in fire safety or health impacts? Organohalogen Compds. 74: 1513-1516.

Chandra, A. K. and V. Sreedhara Rao (1997). Two-dimensional tunneling of hydrogen in a norrish type ii process of a ketone. Chem. Phys. Lett. 270: 87-92.

da Silva, G. and J. W. Bozzelli (2008). Variational analysis of the phenyl + O_2 and phenoxy + O Reactions. J. phys. Chem. A. 112: 3566-3575.

Davis, E. F., S. L. Klosterhaus and H. M. Stapleton (2012). Measurement of flame retardants and triclosan in municipal sewage sludge and biosolids. Environ. Int. 40(0): 1-7.

Frisch et al, M. J. (2009). Wallingford CT, Gaussian, Inc.

Hites, R. (2005). Brominated flame retardants in the environment J. Environ. Monit. 7: 1033-1036.

Klippenstein, S. J. (2003). RRKM theory and its implementation. Comprehensive Chemical Kinetics. N. J. B. Green, Elsevier. Volume 39**:** 55-103.

Luijk, R. and H. A. J. Govers (1992). The formation of polybrominated dibenzo-p-dioxins (PBDDs) and dibenzofurans (PBDFs) during pyrolysis of polymer blends containing brominated flame retardants. Chemosphere. 25: 361-374.

Mokrushin, V. B., V.; Tsang, W.; Zachariah, M.; Knyazev, V (2002). Gaithersburg, MD, NIST.

O'Keefe, P. W. (1987). Formation of brominated dibenzofurans from pyrolysis of the polybrominated biphenyl fire retardant, firemaster FF-1. Environ. Health Perspect. 23: 347-350.

Thoma, H., G. Hauschulz and O. Hutzinger (1987). PVC-induced chlorine-bromine exchange in the pyrolysis of polybrominated diphenyl ethers, -biphenyls, -dibenzodioxins and dibenzofurans. Chemosphere. 16: 297-307.

Thuan, N. T., N. T. Dien and M. B. Chang (2013). PCDD/PCDF behavior in low-temperature pyrolysis of PCP-contaminated sandy soil. Sci. Total. Environ. 443: 590-596.

Wäger, P. A., M. Schluep, E. Müller and R. Gloor (2011). RoHS regulated substances in mixed plastics from waste electrical and electronicequipment. Environ. Sci. Technol. 46: 628-635.

Weber, R. and B. Kuch (2003). Relevance of BFRs and thermal conditions on the formation pathways of brominated and brominated–chlorinated dibenzodioxins and dibenzofurans. Environ. Int. 29: 699-710.

Wei, H., A. C. Aziz-Schwanbeck, Y. Zou, M. B. Corcoran, A. Poghosyan, A. Li, K. J. Rockne, E. R. Christensen and N. C. Sturchio (2012). Polybromodiphenyl ethers and decabromodiphenyl ethane in aquatic sediments from southern and eastern arkansas, united states. Environ. Sci. Technol. 46: 8017-8024.

Yang, Y., Q. Huang, Z. Tang, Q. Wang, X. Zhu and W. Liu (2012). Deca-brominated diphenyl ether destruction and PBDD/F and PCDD/F emissions from coprocessing deca-bde mixture-contaminated soils in cement kilns. Environ. Sci. Technol. 42: 13409–13416.

Yu, W., J. Hu, F. Xu, X. Sun, R. Gao, Q. Zhang and W. Wang (2011). Mechanism and direct Kinetics study on the homogeneous gas-phase formation of PBDD/Fs from 2-BP, 2,4-DBP, and 2,4,6-TBP as precursors. Environ. Sci. Technol. 45: 1917-1925.

Zacharewski, T., M. Harris, S. Safe, H. Thoma and O. Hutzinger (1988). Applications of the in vitro aryl hydrocarbon hydroxylase induction assay for determining “2,3,7,8-tetrachlorodibenzo-*p*-dioxin equivalents”. Toxicol. 51: 177-189.

Zhao, Y., N. E. Schultz and D. G. Truhlar (2006). Design of density functionals by combining the method of constraint satisfaction with parametrization for thermochemistry, thermochemical kinetics, and noncovalent interactions. J. Chem. Theor. Comput. 2: 364-382.

Table 1: Fitted Arrhenius parameters for all reactions involved in the oxidation of 2,2'-DBB at the high-pressure limit and the temperature range of 300 K to 2000 K.

	Forward			Reverse		
Reaction	A (s^{-1} or cm^3 $molecule^{-1}$ s^{-1})	n	Ea/R (1/K)	A (s^{-1} or cm^3 $molecule^{-1}$ s^{-1})	n	Ea/R (1/K)
M3 → M6	3.02×10^{12}	0.24	13 000	2.09×10^{12}	0.19	34 000
M6 → M8	2.88×10^{11}	0.16	14 000	1.70×10^{12}	0.39	19 600
M7 → M9	2.24×10^{11}	0.70	35 4000	1.70×10^{12}	0.19	14 200
M9 → M10	2.57×10^{12}	-0.14	2 000	6.76×10^{12}	0.00	18 200
M8 → M10	1.95×10^{12}	0.40	15 800	2.81×10^{12}	0.00	26 000
M10 → OH + 1-MBDF	1.17×10^{13}	0.18	6 800	9.55×10^{-11}	0.00	3 000
M7 → Br + M11	1.00×10^{11}	0.28	16 500	1.41×10^{-11}	0.00	17 600
M12 → OBr + DF	4.37×10^{12}	0.19	8 000	7.58×10^{-11}	0.00	6 000
M2 → M4	2.95×10^{11}	0.24	24 000	1.54×10^{12}	0.04	32 200
M2 → M5	3.89×10^{11}	0.33	13 500	1.00×10^{13}	0.03	3 900
M2→ M3	8.51×10^{10}	0.26	11 200	2.69×10^{11}	0.00	6 000
M13 → M14	7.59×10^{11}	0.06	13 500	5.24×10^{12}	0.14	8 300
M13 → Br + DF	4.90×10^{11}	0.14	15 200	1.38×10^{-18}	2.00	16 000
M14 → H + 1-MBDD	2.34×10^{8}	0.86	11 900	1.54×10^{-13}	0.00	5 000
M13 → M15	8.13×10^{11}	0.43	24 200	5.24×10^{12}	0.15	8 400
M3 → M7	2.95×10^{12}	0.29	12 000	1.02×10^{12}	0.26	31 900
M12 → Br + M11	2.29×10^{13}	0.07	11 500	1.94×10^{-16}	1.66	3 200
$O_2 \sum_g^3$ + 2,2'-DBBB → Br + M2	2.95×10^{-23}	2.78	20 500	8.31×10^{-19}	1.94	1 300

Table 2: Arrhenius rate parameters (in temperature range 300 K – 2000 K) for major reactions in the formation of DF and 1-MBDF from oxidation of 2,2'-DBB at 1.0 atm as predicted from RRKM simulations.

Reaction	A (s^{-1} or cm^3 $molecule^{-1}$ s^{-1})	n	Ea/R (1/K)
M2 → M3	2.51×10^{40}	-8.77	15 500
M3 → M7	2.58×10^{41}	-8.90	15 900
M3 → M6	2.29×10^{43}	-9.63	17 400
M2 → M4	3.16×10^{45}	-11.77	24 000
M2 → M5	7.76×10^{40}	-9.14	17 000
M13 → Br + DF	3.98×10^{31}	-6.14	18 400
M13 → M14	1.23×10^{29}	-10.65	16 200
M13 → M15	1.20×10^{47}	-3.15	29 700
M14 → H + 1-MBDD	1.86×10^{21}	-5.33	14 000
M6 → M8	2.57×10^{28}	-23.08	16 400
M8 → M10	1.73×10^{88}	0.53	30 300
M37 → M9	2.96×10^{11}	0.29	35 500

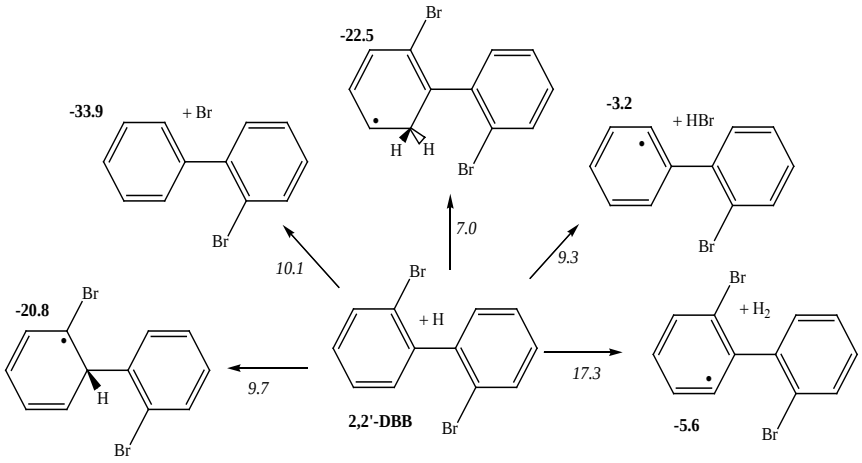

Fig. 1. Reactions of H atoms with the 2,2'-DBB molecule. Values (kcal/mol) in bold and italic are reaction and activation energies, respectively (at 0 K).

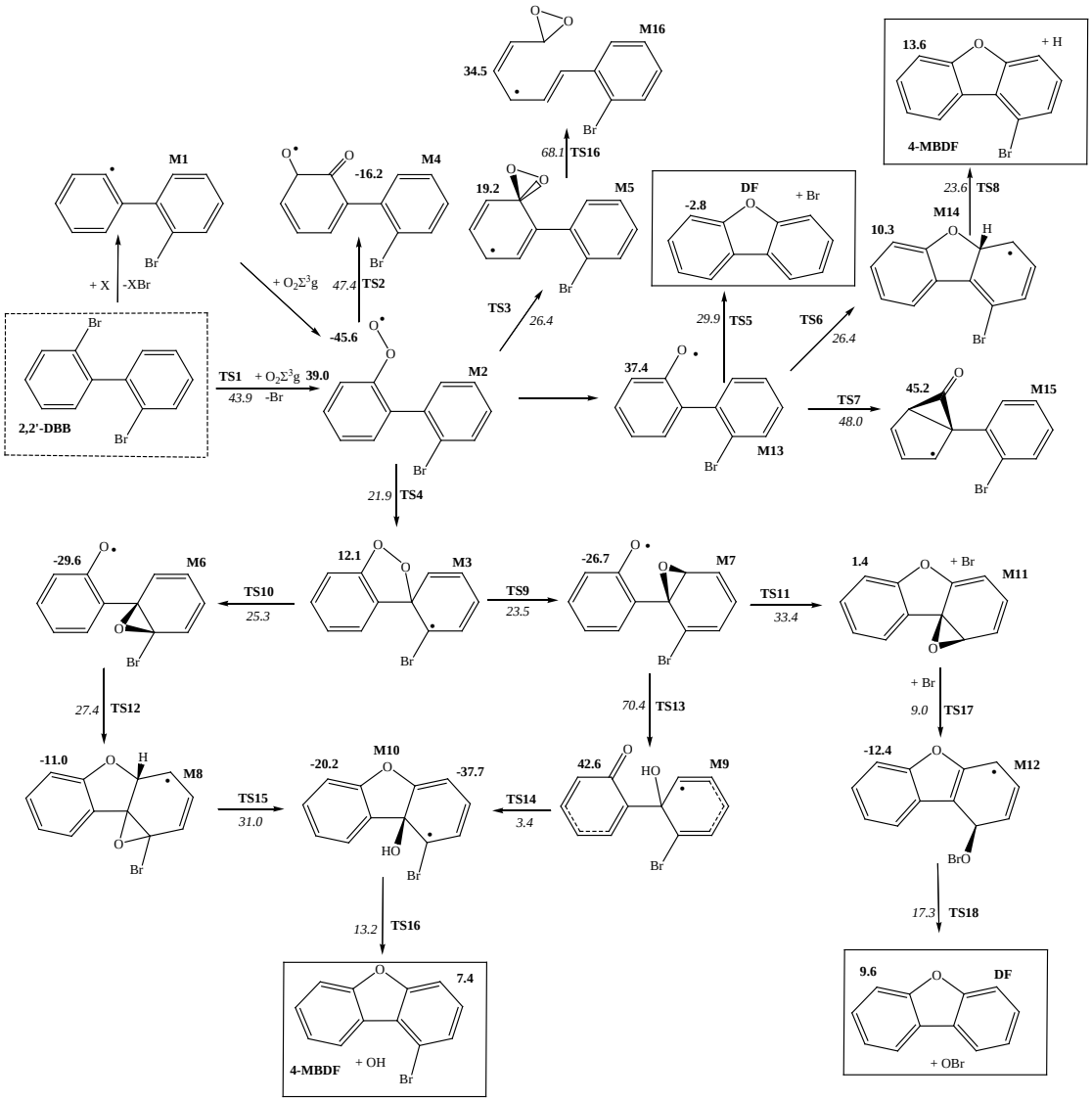

Fig. 2. Formation of **DF** and **1-MBDF** from oxidation of **2,2'-DBB**. Values (kcal/mol) in bold and italic are reaction and activation energies, respectively (at 0 K).

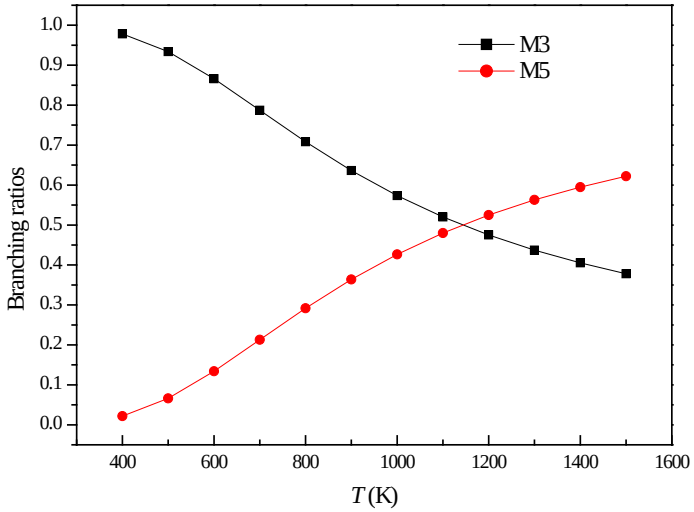

Fig. 3. Branching ratios for isomerisation of M2 into M3 and M5.

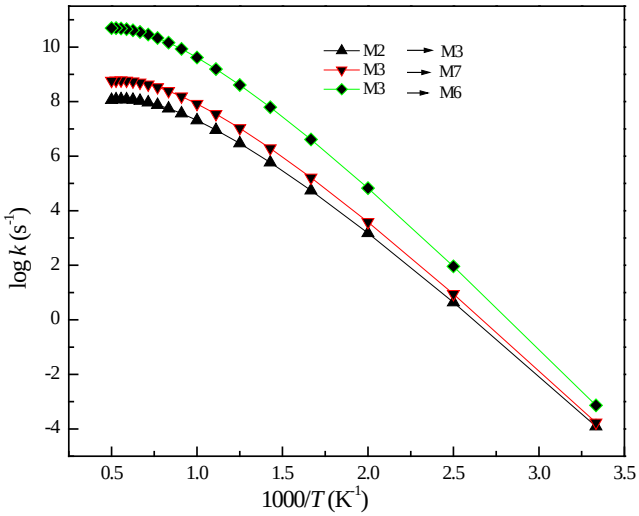

Fig. 4. Arrhenius plots at 1.0 atm for the three opening reactions in the conversion of 2,2'-DBB into DF and 1-MBDF, M2 → M3, M3 → M6 and M3 → M7.